Cooperative catalysis of metal and acid functions in Re-HZSM-5 catalysts for ethane dehydroaromatization

Lei Ma[a,*], Xiaoqin Zou[a,b,*]

[a] Department of Chemical and Biomolecular Engineering, University of California at Berkeley, Berkeley, CA, 94720, United States
[b] Faculty of Chemistry, Northeast Normal University, Changchun, 130024, China

ABSTRACT

A vapor-phase exchange method was used for the encapsulation of Re metal clusters in dehydrated HZSM-5 zeolites with Brønsted acid O−H groups. The reaction pathway of ethane non-oxidative dehydroaromatization on Re-HZSM-5 catalysts was revealed by an experimental observation of the contact time effects on hydrocarbon product selectivity. The reaction pathway typically includes the dehydrogenation of ethane to form olefin reactant pool *via* ethylene formation and immediate dimerization to butene, further dehydrogenation of ethylene to acetylene, and eventual formation of benzene products. The possible elementary step of ethane non-oxidative dehydroaromatization was revealed by kinetic measurements of the dependence of ethane and hydrogen pressures on the turnover rates of benzene formation. The kinetic observation indicates that the dehydrogenation of ethylene to acetylene is the rate-determining step that mediates the whole reaction event. Cooperative catalysis of metal and acid functions is observed on Re-HZSM-5 catalysts. Re metal clusters contribute to ethane activation and formation of initial alkene intermediates. The acid sites would further promote the oligomerization and cyclization reaction and generate benzene and toluene. The bifunctional pathways involving metal and acid roles in ethane non-oxidative dehydroaromatization were further studied on Re-HZSM-5, HZSM-5, and Re-SIL-1/HZSM-5 catalysts. The site proximity between Re metal clusters and acid sites plays a critical role in benzene formation, exemplified by initial rates of benzene formation of 0.03 and 0.43 μmol(C) g_{cat}^{-1} s^{-1} on Re-SIL-1/HZSM-5 and Re-HZSM-5 catalysts, respectively. These two catalysts contain long and short distances of approximately 75 and 1.3 nm between Re metals and acid domains.

1. Introduction

Aromatics and ethylene are important elementary petrochemicals and widely used in the chemical industry, which provides the driving force for the development of ethane dehydroaromatization. Non-oxidative dehydroaromatization *via* high-temperature pyrolysis has been recognized as one efficient route of the conversion of light alkanes to value-added compounds like aromatics [1,2]. To date, Ga/HZSM-5 [3–6], Zn/HZSM-5 [7], and Mo/HZSM-5 [8–19] catalysts have proven to be effective for the dehydroaromatization reaction of light alkanes. These bifunctional catalysts containing two separate functionalities (*e.g.*, metal centers and zeolite solid acids) were usually considered for the dehydroaromatization reaction, because metal center and solid acid functions play different catalytic roles for activation and dehydrogenation of alkane reactants. For this reason, the chemical status of metal species and the properties of the microporous zeolite materials (*e.g.*, the acidity and pore structure) are critical for the

dehydroaromatization reactions. Several catalytic data are available for ethane dehydroaromatization using zeolite supported gallium, zinc, platinum, and molybdenum catalysts [20–26], which include both metal dehydrogenation sites and acid aromatization sites. The major research topics are to determine the precise roles of metal and acid sites, the reaction mechanism of the aromatization of ethane, and the catalyst stability and deactivation.

Re-HZSM-5 catalysts have been reported to effectively catalyze the dehydroaromatization reaction of light alkane [27–29]. In this study, Re-HZSM-5 catalysts were chosen as the ethane non-oxidative dehydroaromatization catalysts. Re is selected as our targeted metal because of its well-defined structure of metallic nanoparticles, while HZSM-5 solid acid is chosen to support Re clusters due to its unique crystalline structure with aperture size of 0.55 nm, which might be beneficial for the selective production of benzene due to the similarity of pore size with the kinetic diameter of benzene (0.5 nm). HZSM-5 supports could also exhibit high thermal stability and offer flexibility to vary Brønsted

acid densities by changing Al contents in MFI frameworks. In this study, Re-HZSM-5 catalysts were prepared by a sublimation method using the vapor-phase exchange of Re_2O_7 with Brønsted acid O—H groups in the dehydrated HZSM-5 zeolite. The possible elementary step of ethane non-oxidative dehydroaromatization reaction was revealed by kinetic measurements of the dependence of ethane and hydrogen pressures on the turnover rates of benzene formation. Also, the functions of metal and acid for ethane non-oxidative dehydroaromatization and the structure-reactivity relationship were proposed. We are trying to correlate Re metal and acid densities with turnover rates of benzene formation on Re-HZSM-5. The dehydroaromatization reaction appears to proceed *via* a bifunctional pathway. Metal species is responsible for the alkane activation and formation of the alkene intermediates. The oligomerization and cyclization catalyzed over acid sites of alkene intermediates would generate benzene, toluene, and naphthalene. The results and conclusions will help us to comprehensively understand the reaction chemistry and the bifunctional catalysis of ethane non-oxidative dehydroaromatization.

2. Experimental methods

2.1. Re-HZSM-5 catalyst synthesis

The Re-HZSM-5 sample preparation protocols are described below, which is referred to the procedures in the literature with some modifications and improvements [28,29]. NH_4-ZSM-5 (Si/Al = 11.5, 15, 25, 40, Zeolyst International) were treated with a flow of dry air (1.67 $cm^3 g^{-1} s^{-1}$, Praxair, 99.999%) to 773 K (0.0167 K s^{-1}) for 5 h to yield HZSM-5. To remove adsorbed H_2O, the obtained HZSM-5 and Re_2O_7 crystalline (Sigma-Aldrich, 99.9%) were treated in ampules under vacuum for 16 h at 573 K and 413 K, respectively. Dried Re_2O_7 and HZSM-5 were mixed together in stagnant N_2 by using an agate mortar and pestle, and ground for approximately 0.5 h to form homogenous physical mixtures of Re_2O_7 and HZSM-5. The intimate mixtures containing Re_2O_7 and HZSM-5 were heated to 723 K (0.083 K s^{-1}) within a quartz reactor in dry air (1.67 $cm^3 g^{-1} s^{-1}$, Praxair, 99.999%) and held for 3 h. Before cooling down to ambient temperature, the corresponding samples were purged in a flow of He (1.67 $cm^3 g^{-1} s^{-1}$, Praxair, 99.999%) for 0.3 h and then reduced directly in H_2/He flow (20 kPa H_2, 1.67 $cm^3 g^{-1} s^{-1}$) at 773 K for 3 h without any exposure to ambient air. The Re_2O_7 exchange and reduction pathways are given in Scheme S1. Re_2O_7 vapor was exchanged with acidic protons in HZSM-5 crystals at elevated temperatures. The replacement of protons by ReO_x species could presumably guarantee small Re clusters within HZSM-5 crystals after ReO_x reduction, because most protons located in the intersections of HZSM-5 channels. It is speculated that metallic Re clusters are the active sites for ethane dehydrogenation, which should be different from Mo/ZSM-5 and Cr/ZSM-5 catalysts [19,30].

For comparison, Re-silicalite-1 (pure silica MFI zeolite) catalysts were also synthesized in this study. The synthesis of silicalite-1 zeolite (denoted as SIL-1) followed the procedures reported in the literature [31], and Re-SIL-1 were prepared by the same vapor-phase exchange method as described above. This preparation method led to Re-SIL-1 catalysts having a typical MFI zeolite structure with a surface area of 228 $m^2 g^{-1}$, micropore volume of 0.11 $cm^3 g^{-1}$, and Re cluster size of 1.4 nm (as shown in Fig. S1). The elemental compositions of all the samples were obtained by inductively coupled plasma atomic emission spectroscopy (ICP-AES) from Galbraith Laboratories.

2.2. Characterization methods

Micromeritics 3Flex Surface Characterization Analyze was used to measure the N_2 adsorption-desorption isotherms of different samples at the temperature of liquid N_2 (77 K). Before the experiment, the samples were pretreated in vacuum at 473 K for 10 h. The specific surface area was determined from the linear portion of the BET plot. The pore size distribution was calculated using the t-plot method.

Transmission electron microscopy (TEM) was performed on a FEI Tecnai G^2 F20 S-TWIN with an acceleration voltage of 200 kV. Metal cluster size distributions were determined by counting at least 400 crystallites. The surface-area weighted cluster diameters, d_{TEM}, were calculated using $d_{TEM} = \sum n_i d_i^3 / \sum n_i d_i^2$, where n_i is the number of metal clusters with a diameter d_i. Before the tests, a small amount of the catalysts was ground by an agate mortar, diluted in acetone and further dispersed by ultrasonication, and then dropped onto a copper grid-supported carbon film.

X-ray diffraction (XRD) measurement was carried out on a Bruker D8 X-ray diffractometer instrument using Cu Kα radiation (λ = 1.54178 Å) at 40 kV and 40 mA under ambient conditions. The scan angle extended from 5° to 50° using a step size of 0.02°, and the accumulated data at a rate of 0.04° s^{-1}.

The average Re cluster diameter was measured from volumetric uptakes of O_2, irreversibly chemisorbed on Re clusters at 303 K. The samples were firstly heated to 773 K at a ramp rate of 0.05 K s^{-1} in flowing H_2 (Praxair, 99.999%, 1.67 $cm^3 g^{-1} s^{-1}$) and held for 3 h, and then evacuated by roughing pump for 1 h at 773 K to remove any adsorbed hydrogen. When the temperature decreased to 303 K in a vacuum condition, O_2 adsorption isotherms were measured at 303 K between 0 and 100 kPa of O_2. Two isotherms were measured consecutively, and the samples were evacuated under a dynamic vacuum for 0.5 h between these measurements. The fractions of exposed Re atoms were determined from the difference between extrapolated values from the isotherms to zero O_2 pressure and by assuming O-to-surface Re adsorption stoichiometry of 0.5. The representative O_2 adsorption isotherms on Re-HZSM-5 catalysts are shown in Fig. S2.

2.3. Ethane dehydroaromatization and product selectivity

Ethane dehydroaromatization tests were performed on Re-HZSM-5 samples using a quartz reactor with plug-flow dynamics. Prior to the measurement, catalyst powders were pelletized and sieved to retain an aggregate diameter of 0.125–0.177 mm. The prepared samples (0.5 g) loaded in a fritted quartz reactor (8 mm diameter) were pretreated by hydrogen (20% H_2/He, 1.67 $cm^3 g^{-1} s^{-1}$, Praxair, 99.999%) from 298 K to 773 K (0.083 K s^{-1}), and then switched to He (1.67 $cm^3 g^{-1} s^{-1}$, Praxair, 99.999%) to remove any residual H_2 in the reactor. The pretreated catalysts were exposed to ethane (50% C_2H_6/Ar, Praxair, 99.999%) with Ar as a balance gas at 773 K. The total pressure of all the gases is standard atmospheric pressure (1.01325×10^5 Pa). Reactant and product concentrations in the effluent stream were measured by gas chromatography (Agilent 6890) through transfer lines maintained at 453 K. Hydrocarbons were separated using a methyl silicone capillary column (HP-1; 50 m × 0.25 mm, 0.25 μm film thickness) connected to a flame ionization detector. C_2H_6, H_2, and Ar (as internal standard) were separated by a Porapak Q packed column (80/100 mesh, 1.82 m × 3.2 mm) with a thermal conductivity detector.

3. Results and discussion

3.1. Structural features of Re-HZSM-5 samples

Table 1 summarizes the effect of Re loading on Re cluster size and pore structure of as-prepared Re-HZSM-5 samples with Si/Al = 15. The TEM images and the Re metal cluster distributions are shown in Figs. S3 and S4, respectively. It is observed that d_{TEM} and d_{chem} values are similar for Re-HZSM-5 samples with low Re/Al_f value (< 0.18). The chemisorption uptakes of O_2 gave higher dispersions of Re metal clusters in HZSM-5 indicating small Re clusters formation, while small surface-averaged mean cluster diameter (d_{TEM} = 1.6–2.2 nm) could be also observed by TEM images. Meanwhile, for Re-HZSM-5 samples with higher Re loading (Re/Al_f > 0.36), Re cluster diameter detected by d_{TEM} and d_{chem} obviously increased, suggesting the agglomeration of Re

Table 1

Metal content, dispersion, mean cluster diameter, and BET surface area, and micropore volume of different HZSM-5 and Re-HZSM-5 samples.

Sample	Re/Al$_f$ [a]	Si/Al[b]	Dispersion[c]	d$_{chem}$ (nm)[d]	d$_{TEM}$ (nm)[e]	BET surface area (m^2 g^{-1})[f]	Micropore volume (cm^3 g^{-1})[g]
HZSM-5	–	15	–	–	–	416.8	0.14
Re-HZSM-5	0.05	15	0.85	1.6	1.6	372.1	0.14
Re-HZSM-5	0.09	15	0.71	1.9	2.1	230.8	0.14
Re-HZSM-5	0.18	15	0.65	2.1	2.2	220.8	0.14
Re-HZSM-5	0.36	15	0.29	4.7	4.4	195.0	0.13
Re-HZSM-5	0.90	15	0.18	7.6	6.3	297.0	0.14

[a] Determined from ICP-AES.
[b] The Si/Al value is quoted from reference [32].
[c] Determined from O$_2$ chemisorption.
[d] Estimated by the Re dispersion using $d_{chem} = 6 \times \frac{v_m / a_m}{D}$, where v$_m$ is the volume of an atom in the bulk of Re metal (15.06×10^{-3} nm^3), and a$_m$ is the surface area occupied by an atom on a polycrystalline surface of Re (6.60×10^{-2} nm^2) [33].
[e] Determined from TEM analysis, $d_{TEM} = \sum n_i d_i^3 / \sum n_i d_i^2$.
[f] Determined from N$_2$ adsorption-desorption isotherms.
[g] Determined by a t-plot method from N$_2$ adsorption-desorption isotherms.

particles over high Re loading samples. It should be noted that Re-HZSM-5 samples might appear to contain very small Re clusters, which were difficult to be detected by the TEM images at this magnification level. Therefore, d$_{chem}$ value was used to calculate the turnover rate, because it includes all the Re metal clusters present and directly depends on the surface metals to adsorb the reactants.

The dispersity index (DI) is used to describe Re cluster distribution. The DI value is defined as the surface-averaged diameter ($d_{TEM} = \sum n_i d_i^3 / \sum n_i d_i^2$) divided by the number-averaged diameter ($d_{TEM} = \sum n_i d_i / \sum n_i$), where n$_i$ is the number of metal clusters with a diameter d$_i$. This parameter with a value of unity is corresponding to unimodal clusters and the values smaller than 1.5 is ascribed to relatively uniform size distributions. As shown in Fig. 1, the DI value for Re-HZSM-5 samples with Re/Al$_f$ value lower than 0.18 was near unity (1.17–1.27), which was consistent with narrow size distributions of Re clusters on these samples. The size uniformity and mean cluster diameters detected by TEM images might suggest that Re metal clusters were encapsulated within the HZSM-5 crystals. The DI value increased to 1.57 when Re loading increased to Re/Al$_f$ = 0.90, indicating agglomerated Re particles formed over the HZSM-5 crystal surface with this high Re loading.
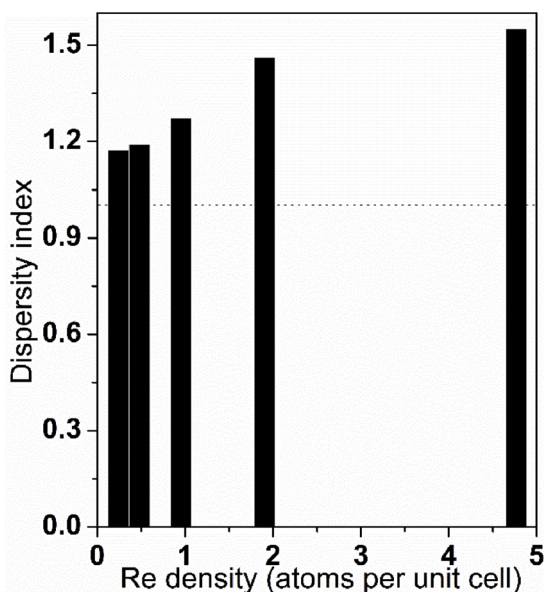
As shown in Fig. 2, type I isotherms of N$_2$ physical adsorption are observed on pure HZSM-5 and Re-HZSM-5 catalysts, suggesting that the microporous structures are intact after introducing Re clusters. BET surface area and pore volume of pure HZSM-5 supports were 416.8 m^2 g^{-1} and 0.14 cm^3 g^{-1}, and decreased to 195.0 m^2 g^{-1} and 0.13 cm^3 g^{-1} of Re-HZSM-5 catalysts with Re/Al$_f$ = 0.36. Obviously, the BET surface area would decrease with the introduction of Re, and the micropore volume slightly decreased in comparison with pure HZSM-5 supports. The N$_2$ adsorption-desorption results indicated that the encapsulated Re clusters probably occupied the pore spaces by slightly shattering the local environments but without destroying the whole zeolite structure. It should be noted that the amount of N$_2$ adsorption and the BET surface area of Re-HZSM-5 samples with Re/Al$_f$ = 0.90 was higher than the corresponding value of the sample with Re/Al$_f$ = 0.36. This result suggests that Re particles would prefer to form over HZSM-5 crystal surface, but not be fully encapsulated into the micropores when Re loading was too high.

Fig. 1. Dispersity index of Re clusters from TEM images.
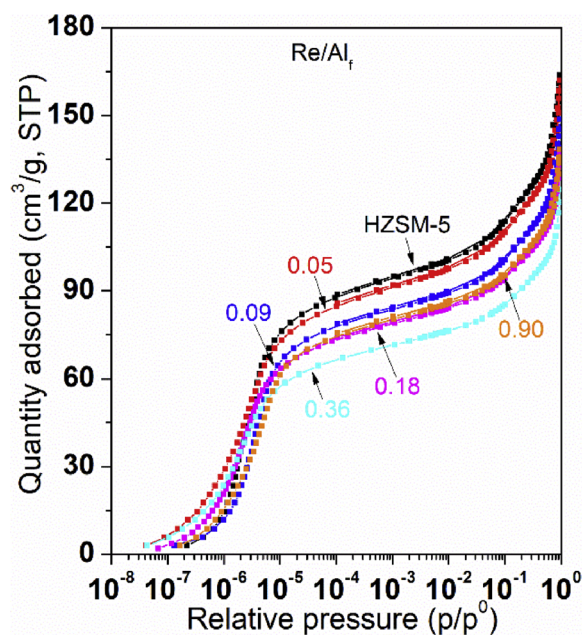
Fig. 2. N$_2$ adsorption-desorption isotherms of HZSM-5 and different Re-HZSM-5 catalysts.

3.2. Ethane dehydroaromatization and selectivity on Re-HZSM-5

As shown in Fig. 3, the approach-to-equilibrium values (η) are defined as Eqs. (1) and (2), where K_{eq} is the equilibrium constant, and $[H_2]$, $[C_2H_4]$, and $[C_4H_8]$ represent the relative partial pressures of each of species ($[A] = p_A/p_0$, where A = H_2, C_2H_4, or C_4H_8, and p_0 is the total pressure (1.01325×10^5 Pa)). The η value for ethane to ethylene and ethylene to butene were approximately between 0.8 and 1.0 in this study. Therefore, ethane, ethylene, and butene could be essentially treated as a single chemical species (reactant pool) because of this proximity of η to unity. It should be noted that constant hydrogen (7 kPa) was fed into the reactor in the test, which could facilitate the chemical equilibrium of C_2H_6 and C_2H_4 with varying the residence time. Generally, after ethylene was formed *via* dehydrogenation of ethane over Re sites, it would be equilibrated with butene instantly, which could be recognized as a "lumped reaction pool". Thus, the pool conversions were used instead of the single ethane conversion. In addition, the approach-to-equilibrium values of ethane or ethylene to the other species (*e.g.*, CH_4, C_3H_6, C_3H_8, C_6H_6, and C_7H_8) were below 0.2, suggesting these hydrocarbons should be the reaction products during the dehydroaromatization process.
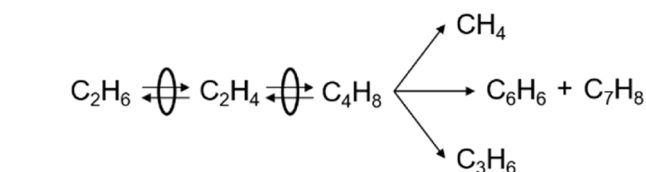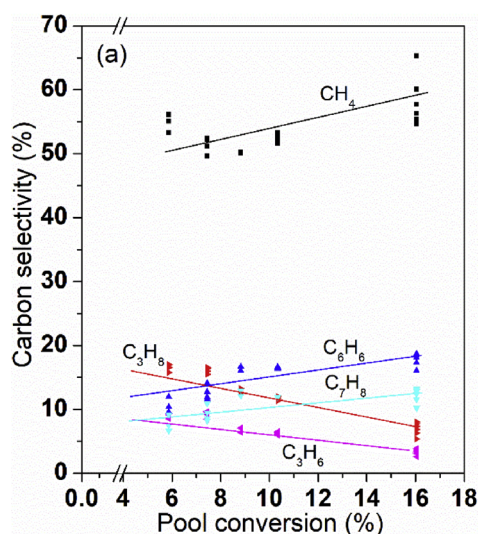
Scheme 1. Reaction pathways for ethane dehydroaromatization on Re-HZSM-5 catalysts.

3.3. Effects of C_2H_6 and H_2 pressures on turnover rates of benzene formation

The reaction kinetics were evaluated by studying the dependence of ethane and hydrogen pressures on the turnover rates of benzene formation. The mean partial pressures ($p_{C_2H_6}$ and p_{H_2}) are reported as the linear average of the inlet and outlet pressures (Eqs. (3) and (4)):

$$p_{C_2H_6} = \frac{p_{C_2H_6,inlet} + p_{C_2H_6,outlet}}{2} \tag{3}$$
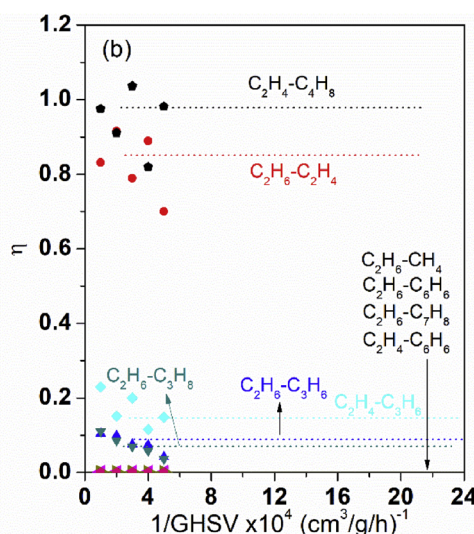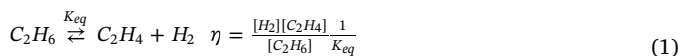

Fig. 3. The relations of carbon selectivity and residence time on Re-HZSM-5 (Re/Al$_f$ = 0.18, Si/Al = 15) at 773 K with constant H_2 (7 kPa), SV = 0.07 ~ 0.41 cm^3(C_2H_6) g$_{cat}^{-1}$ s^{-1}.

$$C_2H_6 \overset{K_{eq}}{\rightleftarrows} C_2H_4 + H_2 \quad \eta = \frac{[H_2][C_2H_4]}{[C_2H_6]} \frac{1}{K_{eq}} \tag{1}$$

$$2C_2H_4 \overset{K_{eq}}{\rightleftarrows} C_4H_8 \quad \eta = \frac{[C_4H_8]}{[C_2H_4]^2} \frac{1}{K_{eq}} \tag{2}$$

It is observed that methane, benzene, and toluene are the predominant products of ethane dehydroaromatization over Re-HZSM-5 (Re/Al$_f$ = 0.18, Si/Al = 15). The selectivity of methane, benzene, and toluene increases with the residence time, indicating that these species are the secondary products. Methane should be the secondary products through the cracking reaction, while the aromatics are formed *via* acid catalyzed oligomerization and cyclization. It is speculated that the lumped pools of ethane, ethylene, and butene would migrate to acid sites and convert to benzene and toluene because of alkene double bond interaction over Brønsted acid sites. Based on the above experimental results, the reaction scheme for ethane dehydroaromatization over Re-HZSM-5 catalysts could be proposed. Scheme 1 depicts a reaction scheme of the ethane dehydroaromatization reaction on the Re-HZSM-5 catalysts.

$$p_{H_2} = \frac{p_{H_2,inlet} + p_{H_2,outlet}}{2} \tag{4}$$

As shown in Fig. 4a, the turnover rates of benzene formation are proportional to the ethane pressures with constant H_2 in the co-feed streams on Re-HZSM-5 catalysts at 773 K. The dependence of benzene formation turnover rates on ethane pressure is calculated to be 1.0, which suggests that unsaturated C2 species should be the reaction intermediates involved in the subsequent step of benzene formation. The involvement of unsaturated C2 species, formed *via* quasi-equilibrated dehydrogenation steps, would play as the reaction intermediates that mediate rate-determining steps [34]. The turnover rates of benzene formation as a function of measured C_2H_4 pressures in the effluent stream are plotted in Fig. 4b. Obviously, the turnover rates of benzene formation are proportional to C_2H_4 pressures in the range of 0.6 to 0.9 kPa. This result further confirms that the C2 related intermediates should take part in the benzene formation. The inserted plot in Fig. 4 indicates the approach-to-equilibrium value for ethane to ethylene is approximately unity in this study.
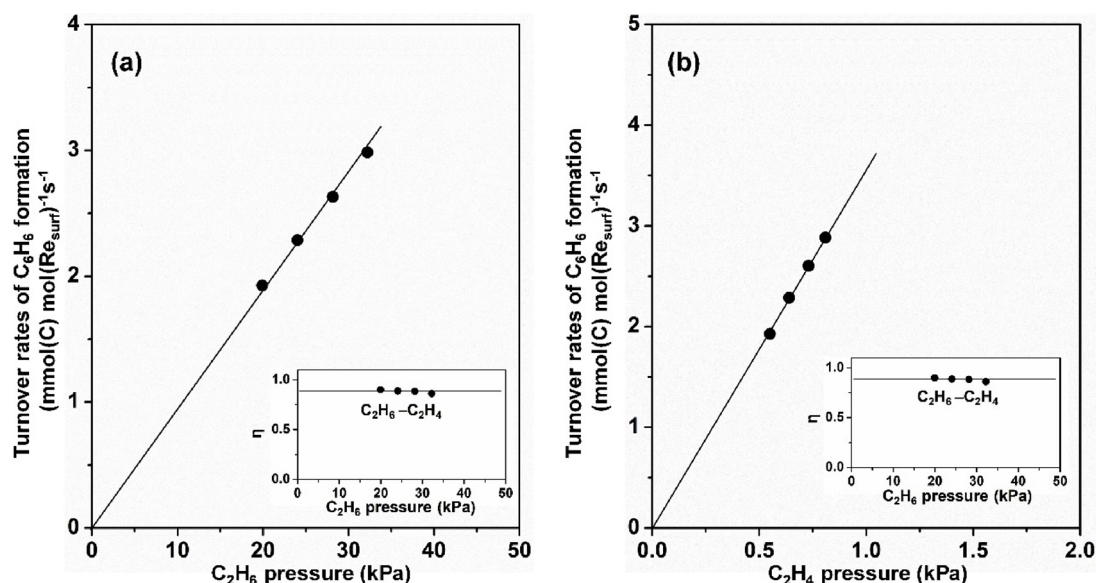
Fig. 4. Turnover rates of benzene formation in function of (a) C_2H_6 pressures (constant 7 kPa H_2, insert shows approach-to-equilibrium of C_2H_6 to C_2H_4) and (b) measured C_2H_4 pressures ($p(C_2H_4) = (p_{inlet} + p_{outlet})/2$) at 773 K on Re-HZSM-5 catalysts (Re/Al$_f$ = 0.18, Si/Al = 15).

As shown in Fig. 5a, the turnover rates of benzene formation are inversely depended on H_2 pressures, while an average of two hydrogen atoms evolves as H_2 $((H_2)^{-0.91})$ during the conversion of lumped reaction pool of C_2H_6-C_2H_4 to C_6H_6, which suggests that the first H abstraction from C_2H_4 to form unsaturated C_2H_3 intermediate should be the rate-determining step. The turnover rates of benzene formation linearly increase with measured C_2H_4 concentrations (0.5–0.7 kPa) in the effluent stream (Fig. 5b), which also confirms that the C2 related intermediates take part in the benzene formation.

the ethane molecule (where * indicates a vacant site on Re cluster surface atom) (2.1 and 2.2). The dehydrogenation of C_2H_4* to form unsaturated C_2H_3* or C_2H_2* species is irreversible and represents the rate-determining steps (2.3 and 2.4) [35]. The surface intermediates (C_2H_4* and C_2H_3*) remove H-atoms with a rate constant that reflects the difficulty of C−H cleavage from C_2H_4* and C_2H_3* species, thus mediates the whole reaction event. Adsorbed H* desorb from the catalyst surface to form gaseous H_2 and release the vacant sites (2.5 and 2.6). The C_2H_2* species further transfer from Re cluster surface sites to
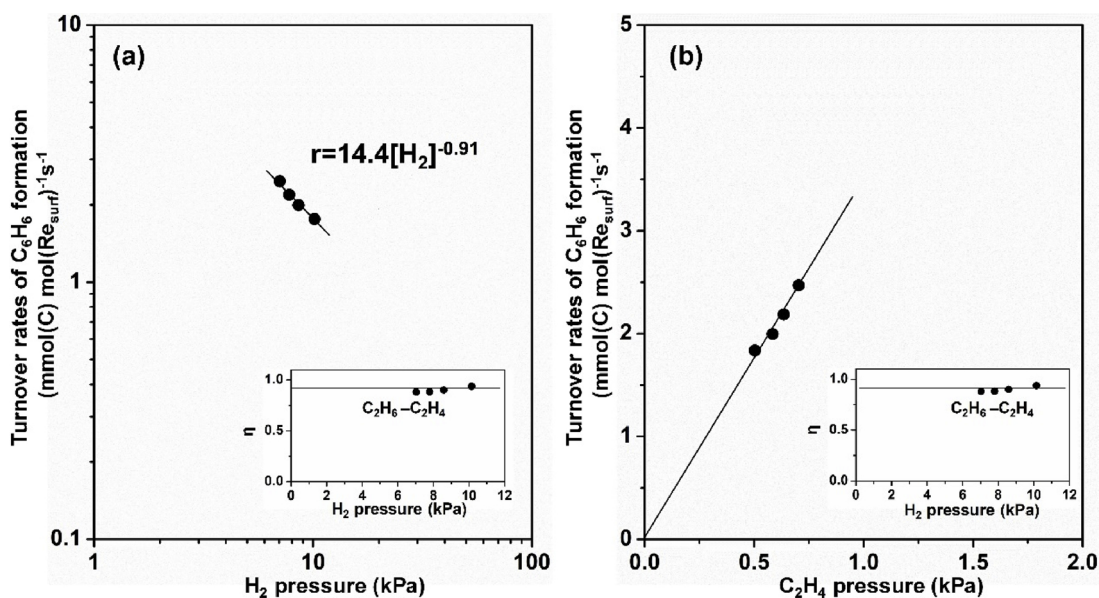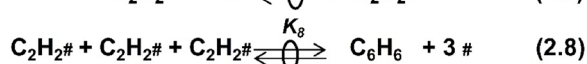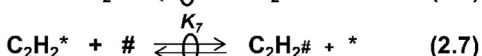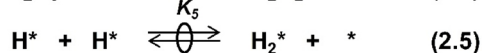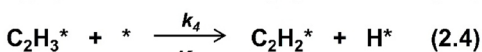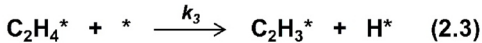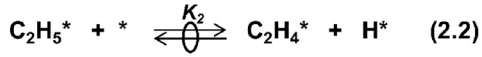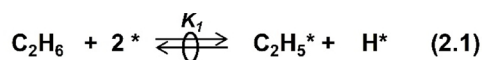

Fig. 5. Turnover rates of benzene formation in function of (a) H_2 pressures (constant 25 kPa C_2H_6, insert shows an approach-to-equilibrium of C_2H_6 to C_2H_4) and (b) measured C_2H_4 pressures ($p(C_2H_4) = (p_{inlet} + p_{outlet})/2$) at 773 K on Re-HZSM-5 catalysts (Re/Al$_f$ = 0.18, Si/Al = 15).

Scheme 2 shows a sequence of elementary steps consistent with the observed kinetic data of ethane and hydrogen pressures that account for the turnover rates of benzene formation (Figs. 4 and 5). The reaction sequence includes molecular C_2H_6 adsorption and C−H bond cleavage of adsorbed C_2H_6 to form a quasi-equilibrated pool of chemisorbed C_2H_4* surface intermediates with two hydrogen atoms removed from

acidic sites to form C_2H_2# (2.7, # indicates a vacant acid site). The presence of equilibrated mixtures of C_2H_4-C_4H_8 during ethane dehydroaromatization on Re-HZSM-5 suggests that the oligomerization of C_2H_4 to long chained alkenes C_4H_8 is quasi-equilibrated over acid sites, which is analogous to the steps for C_2H_2 trimerization (2.8) to form large molecules (e.g., C_6H_6).

$$C_2H_6 + 2\,* \underset{K_1}{\overset{}{\rightleftharpoons}} C_2H_5* + H* \qquad (2.1)$$

$$C_2H_5* + \,* \underset{K_2}{\overset{}{\rightleftharpoons}} C_2H_4* + H* \qquad (2.2)$$

$$C_2H_4* + \,* \overset{k_3}{\longrightarrow} C_2H_3* + H* \qquad (2.3)$$

$$C_2H_3* + \,* \underset{k_4}{\overset{}{\longrightarrow}} C_2H_2* + H* \qquad (2.4)$$

$$H* + H* \underset{K_5}{\overset{}{\rightleftharpoons}} H_2* + \,* \qquad (2.5)$$

$$H_2* \underset{K_6}{\overset{}{\rightleftharpoons}} H_2 + \,* \qquad (2.6)$$

$$C_2H_2* + \# \underset{K_7}{\overset{}{\rightleftharpoons}} C_2H_2\# + \,* \qquad (2.7)$$

$$C_2H_2\# + C_2H_2\# + C_2H_2\# \underset{K_8}{\overset{}{\rightleftharpoons}} C_6H_6 + 3\,\# \qquad (2.8)$$

Scheme 2. The proposed reaction pathways for ethane dehydroaromatization over Re-HZSM-5 catalysts (* is an unoccupied metal surface site; # is an unoccupied acid site; k_x and K_x are rate constant and equilibrium constant, respectively.).

Scheme 2 leads to turnover rates of benzene formation proportional to the concentration of the reactive unsaturated intermediates ($[C_2H_4*]$)

$$r = k_3 \cdot [C_2H_4*] \cdot [*] \qquad (5)$$

in which k_3 is the rate constant of C–H breakage in C_2H_4*, and [*] denotes the coverage of vacant metal surface sites. The assumption of pseudo-steady state for $[C_2H_4*]$ and quasi-equilibrium for step (2.1), (2.2), (2.5), and (2.6) in Scheme 2 lead to Equation (6) for the rate expression of C_2H_6 conversion to C_6H_6 in terms of C_2H_6 and H_2 pressure.

$$r = k_3 K_1 K_2 K_5 K_6 \frac{[C_2H_6][*]^2}{[H_2]} \qquad (6)$$

Here, k_3 is the rate constant for H abstraction from C_2H_4*, K_x is the equilibrium constant for each step, and [*] denotes the coverage of unoccupied metal surface sites. The site balance can be given by: $1.0 = [*] + [C_2H_5*] + [C_2H_4*] + [C_2H_3*] + [C_2H_2*] + [H_2*] + [H*]$, in which the terms labeled as [*], $[C_2H_5*]$, $[C_2H_4*]$, $[C_2H_3*]$, $[C_2H_2*]$, $[H_2*]$, and [H*] represent their respective coverages during catalysis. The maximum value of each species coverage is 1.0. It is assumed that most of the Re metal surface sites are free ([*] = 1.0) at the reaction temperature of 773 K. The application of the quasi-steady-state approximation and site balance gives the following expression for the reaction rate.

$$r = k_3 K_1 K_2 K_5 K_6 \frac{[C_2H_6]}{[H_2]} \qquad (7)$$

The derived rate Eq. (7) is consistent with the experimental turnover rates of benzene formation as shown in Figs. 4a and 5 a. The measured values of reaction power in C_2H_6 and H_2 reflects that the rates of ethylene conversion to benzene are proportional to ethylene pressures in the system, which is consistent with the results in Figs. 4b and 5 b.

3.4. Effects of site proximity on reaction rates

The proximity between metal and acid sites plays an important role in the bifunctional catalysis of heterogeneous catalysis [36]. According to Scheme 2, the transformation of C_2H_2* on Re cluster surface sites to $C_2H_2\#$ on vicinal acidic sites should be critical for benzene formation. To demonstrate the proximity roles of Re metals and zeolite acid sites, HZSM-5, Re-HZSM-5, and Re-SIL-1/HZSM-5 physical mixture samples were tested for ethane dehydroaromatization reaction. The distances between Re metals and acid domains over Re-SIL-1/HZSM-5 and Re-HZSM-5 catalysts are estimated to be approximately 75 and 1.3 nm. The calculation of the distance of Re metals and acid sites are based on the following assumption: for HZSM-5 zeolite (Si/Al = 15, CBV 3024E), the number of H^+ per unit cell ($Al_6Si_{90}O_{192}$) is about 4, while the number of Re metals per unit cell is about 1 (Re/Al_f = 0.18). The space group of MFI zeolite is orthorhombic with a = 20.0900 Å, b = 19.7380 Å, c = 13.1420 Å, and V = 5211 Å^3. It is assumed that H^+ protons are well dispersed in the unit cell, and then it could be estimated that the distance of Re metals and acid domains is about 1.3 nm for Re-HZSM-5. In addition, HZSM-5 zeolite crystal size is about 75 nm based on TEM images. The distance of Re metals and acid domains is estimated to be 75 nm for Re-SIL-1/HZSM-5 samples. The specific roles of metal and acid in ethane dehydroaromatization could be determined by catalytic reaction over the prepared samples. Table 2 summarizes the initial rates of ethane consumption and the initial rates of benzene formation on different samples. It is observed that pure HZSM-5 exhibits a low initial rates of ethane consumption of 0.26 μmol(C) g_{cat}^{-1} s^{-1}. Meanwhile, Re-SIL-1/HZSM-5 mixtures could exhibit a slightly higher initial rates of ethane consumption of 0.70 μmol(C) g_{cat}^{-1} s^{-1}. It should be noted that Re-SIL-1/HZSM-5 mixture would gradually deactivate during the dehydroaromatization reaction process, and the rates of ethane consumption could remain stable at approximately half of the initial rates after 3 h. This result means that Re-SIL-1 in the physical mixture might be easily deactivated by the formation of surface carbon coke, while only HZSM-5 zeolite would contribute to the dehydroaromatization process. For Re-HZSM-5 samples, the rates of ethane consumption greatly increase and could reach 1.64 μmol(C) g_{cat}^{-1} s^{-1}. The results might indicate that the Re cluster sites are mainly responsible for the ethane dehydrogenation process. In addition, pure HZSM-5 and Re-SIL-1/HZSM-5 could reach the same rate of benzene formation of 0.03 μmol(C) g_{cat}^{-1} s^{-1}. This low value implies that alkene intermediates and benzene formation could not easily take place over either Re metal clusters or acid sites, especially when these two sites are far from each other. Meanwhile, the rate of benzene formation would be significantly improved by approximately 14 times over Re-HZSM-5 catalysts, implying that the proximity of Re metal clusters and zeolite acid sites is responsible for oligomerization and cyclization of the alkene intermediates. Therefore, it is speculated that Re metal clusters mainly contribute to the dehydrogenation of ethane, while the proximity of Re metal clusters and zeolite acid sites promotes the benzene formation.

Table 2
The initial rates of C_2H_6 consumption and the initial rates of C_6H_6 formation over different catalysts.

Sample	Re content (% wt.)[a]	Rate of C_2H_6 consumption (μmol(C) g_{cat}^{-1} s^{-1})[b]	Rate of C_6H_6 formation (μmol(C) g_{cat}^{-1} s^{-1})[c]
HZSM-5	–	0.26	0.03
Re-HZSM-5	3.1	1.64	0.43
Re-SIL-1/HZSM-5[d]	1.5	0.70	0.03

[a] Determined by ICP-AES analysis.
[b] The initial rates of C_2H_6 consumption are calculated at t = 0 s (773 K, 50 kPa C_2H_6, space velocity of 0.30 cm^3(C_2H_6) g_{cat}^{-1} s^{-1}).
[c] The initial rates of C_6H_6 formation are calculated at t = 0 s (773 K, 50 kPa C_2H_6, space velocity of 0.30 cm^3(C_2H_6) g_{cat}^{-1} s^{-1}).
[d] The weight ratio of Re-SIL-1 to HZSM-5 is 1.0 to mix the samples, and the space velocity was kept the same as Re-HZSM-5 catalysts in the kinetic studies.

3.5. Effects of Re metal and acid functions

It is recognized that Re-HZSM-5 catalysts exhibit bifunctional roles in catalytic reactions for alkane dehydroaromatization [27,29]. For ethane dehydroaromatization reaction, Re metal clusters contribute to ethane activation and formation of initial alkene intermediates. Meanwhile, the acid sites would further promote the oligomerization and cyclization reaction and generate benzene and toluene. Here, the separate roles of Re cluster and zeolite acid functions on the forward rates of ethane consumption and the turnover rates of benzene formation were further investigated by varying the Re loading and H^+ proton densities, and the catalytic results are summarized in Fig. 6. As shown in Fig. 6a, both the forward rates of ethane consumption and the turnover rates of benzene formation do not change with varying Re loading. It should be noted that both rates were normalized by Re cluster surface atoms. It implies that the ethane dehydrogenation and benzene formations are not structurally sensitive with the Re cluster sizes, while the Re cluster surface atoms would be responsible for the ethane dehydrogenation and benzene formation. Fig. 6b summarizes turnover rates of benzene formation on series of Re-HZSM-5 catalysts with different acid densities (Si/Al = 11.5, 15, 25, 40; and Re contents were kept at 3.1% wt.). Obviously, the turnover rates of benzene formation have a linear relationship with the acid density, which means that the alkene oligomerization and cyclization to benzene would take place over the acid sites.

4. Conclusions

In this study, isolated and stable Re metal clusters were successfully obtained by the thermal treatment of Re_2O_7 and HZSM-5 mixture. The bifunctional pathways involving metal and acid roles in ethane non-oxidative dehydroaromatization is proposed on Re-HZSM-5 catalysts. Re metal clusters contribute to ethane activation and formation of initial alkene intermediates. The acid sites would further promote the oligomerization and cyclization reaction and generate benzene and toluene. The site proximity of Re metal clusters and zeolite acid sites significantly contributed to the turnover rates of benzene formation. The kinetics and reaction pathways of ethane dehydroaromatization over the Re-HZSM-5 catalysts have been revealed by the experimental observations. The reaction pathway typically includes the activation of ethane molecules on Re metal clusters to form alkene pool *via* first forming ethylene and its dimerization to butene. The kinetic results clearly revealed that the hydrogen atoms removal from adsorbed C_2H_4 molecule should be the rate-determining step in the whole event of ethane dehydroaromatization reaction. The unsaturated $C_2H_3^*$ or $C_2H_2^*$ species further proceeded oligomerization and cyclization process and finally generated benzene. The results and conclusion based on this study will help us to comprehensively understand the reaction kinetics of the complicated system of ethane dehydroaromatization.
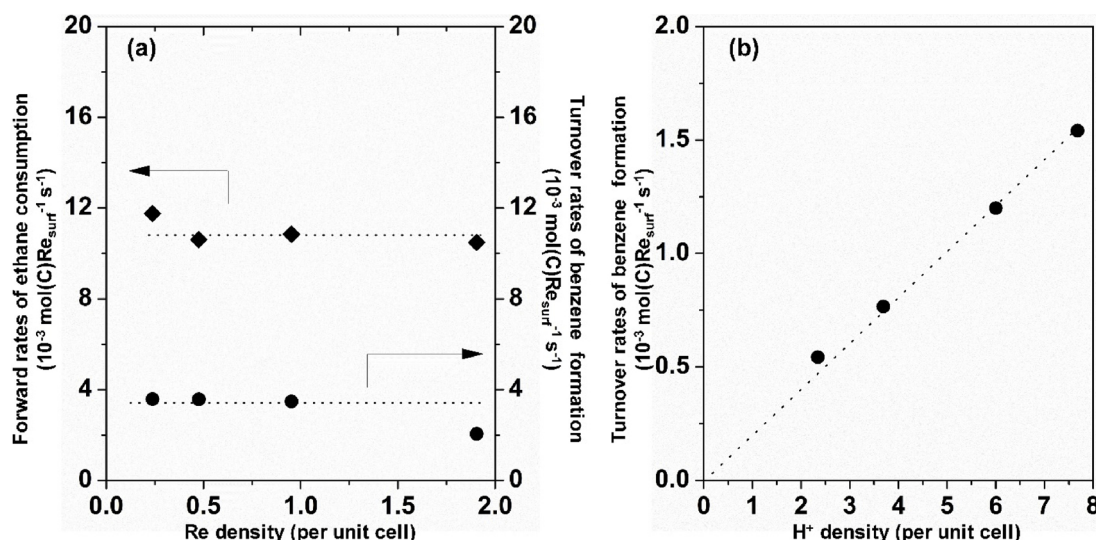

Fig. 6. Initial forward rates of ethane consumption and initial turnover rates of benzene formation in the dependence of (a) Re loading and (b) acid density at t = 0 s (773 K, 50 kPa C_2H_6, space velocity of 0.30 cm³(C_2H_6) g_{cat}^{-1} s^{-1}, and dash lines represent the trends).

The bifunctional roles with separate metal and acid catalytic sites were also studied by feeding ethylene as a reactant for dehydroaromatization reaction. Table S1 shows the ethylene consumption rates and benzene formation rates on HZSM-5, Re-HZSM-5, and Re-SIL-1. It is found that the ethylene consumption rates on Re-HZSM-5 were higher than that on HZSM-5, suggesting that Re metal sites were responsible for activation of C_2H_4 molecules. Additionally, Re-SIL-1 without any acid sites could not generate any benzene during C_2H_4 dehydroaromatization reaction, but only facilitate C_2H_4 dehydrogenation on Re metal sites, suggesting that activation of C_2H_4 on Re metal sites was critical for ethylene dehydrogenation and the acid sites would favor the downward reaction of benzene formation.

Appendix A. Supplementary data

Supplementary material related to this article can be found, in the online version, at doi:https://doi.org/10.1016/j.apcatb.2018.11.014.

References

[1] M. Guisnet, N.S. Gnep, F. Alario, Aromatization of short chain alkanes on zeolite catalysts, Appl. Catal. A Gen. 89 (1992) 1–30.

[2] L. Wang, L. Tao, M. Xie, G. Xu, J. Huang, Y. Xu, Dehydrogenation and aromatization of methane under non-oxidizing conditions, Catal. Lett. 21 (1993) 35–41.

[3] G.L. Price, V. Kanazirev, Ga_2O_3/HZSM-5 propane aromatization catalysts: Formation of active centers via solid-state reaction, J. Catal. 126 (1990) 267–278.

[4] A. Bhan, W. Nicholas Delgass, Propane aromatization over HZSM-5 and Ga/HZSM-5 catalysts, Catal. Rev. 50 (2008) 19–151.

[5] N.M. Phadke, J. Van der Mynsbrugge, E. Mansoor, A.B. Getsoian, M. Head-Gordon, A.T. Bell, Characterization of isolated Ga^{3+} cations in Ga/H-MFI prepared by vapor-phase exchange of H-MFI zeolite with $GaCl_3$, ACS Catal. 8 (2018) 6106–6126.

[6] E. Mansoor, M. Head-Gordon, A.T. Bell, Computational modeling of the nature and role of Ga species for light alkane dehydrogenation catalyzed by Ga/H-MFI, ACS Catal. 8 (2018) 6146–6162.

[7] B.S. Liu, Y. Zhang, J.F. Liu, M. Tian, F.M. Zhang, C.T. Au, A.S.C. Cheung, Characteristic and mechanism of methane dehydroaromatization over Zn-based/HZSM-5 catalysts under conditions of atmospheric pressure and supersonic jet expansion, J. Phys. Chem. C 115 (2011) 16954–16962.

[8] S. Liu, L. Wang, R. Ohnishi, M. Ichikawa, Bifunctional catalysis of Mo/HZSM-5 in the dehydroaromatization of methane to benzene and naphthalene XAFS/TG/DTA/MASS/FTIR characterization and supporting effects, J. Catal. 181 (1999) 175–188.

[9] Y. Xu, X. Bao, L. Lin, Direct conversion of methane under nonoxidative conditions, J. Catal. 216 (2003) 386–395.

[10] B. Yao, J. Chen, D. Liu, D. Fang, Intrinsic kinetics of methane aromatization under non-oxidative conditions over modified Mo/HZSM-5 catalysts, J. Nat. Gas Chem. 17 (2008) 64–68.

[11] J.-P. Tessonnier, B. Louis, S. Rigolet, M.J. Ledoux, C. Pham-Huu, Methane dehydroaromatization on Mo/ZSM-5: about the hidden role of Brønsted acid sites, Appl. Catal. A Gen. 336 (2008) 79–88.

[12] Z.R. Ismagilov, E.V. Matus, L.T. Tsikoza, Direct conversion of methane on Mo/ZSM-5 catalysts to produce benzene and hydrogen: achievements and perspectives, Energy Environ. Sci. 1 (2008) 526–541.

[13] A. Holmen, Direct conversion of methane to fuels and chemicals, Catal. Today 142 (2009) 2–8.

[14] Y. Xu, J. Lu, J. Wang, Y. Suzuki, Z.-G. Zhang, The catalytic stability of Mo/HZSM-5 in methane dehydroaromatization at severe and periodic CH_4–H_2 switch operating conditions, Chem. Eng. J. 168 (2011) 390–402.

[15] Y. Cui, Y. Xu, J. Lu, Y. Suzuki, Z.-G. Zhang, The effect of zeolite particle size on the activity of Mo/HZSM-5 in non-oxidative methane dehydroaromatization, Appl. Catal. A Gen. 393 (2011) 348–358.

[16] C.H.L. Tempelman, E.J.M. Hensen, On the deactivation of Mo/HZSM-5 in the methane dehydroaromatization reaction, Appl. Catal. B: Environ. 176–177 (2015) 731–739.

[17] C. Karakaya, H. Zhu, R.J. Kee, Kinetic modeling of methane dehydroaromatization chemistry on Mo/Zeolite catalysts in packed-bed reactors, Chem. Eng. Sci. 123 (2015) 474–486.

[18] J. Hu, S. Wu, Y. Ma, X. Yang, Z. Li, H. Liu, Q. Huo, J. Guan, Q. Kan, Effect of the particle size of MoO_3 on the catalytic activity of Mo/ZSM-5 in methane non-oxidative aromatization, New J. Chem. 39 (2015) 5459–5469.

[19] J. Gao, Y. Zheng, J.-M. Jehng, Y. Tang, I.E. Wachs, S.G. Podkolzin, Identification of molybdenum oxide nanostructures on zeolites for natural gas conversion, Science 348 (2015) 686–690.

[20] A. Samanta, X. Bai, B. Robinson, H. Chen, J. Hu, Conversion of light alkane to value-added chemicals over ZSM-5/metal promoted catalysts, Ind. Eng. Chem. Res. 56 (2017) 11006–11012.

[21] Z. Ji, H. Lv, X. Pan, X. Bao, Enhanced ethylene selectivity and stability of Mo/ZSM5 upon modification with phosphorus in ethane dehydrogenation, J. Catal. 361 (2018) 94–104.

[22] A. Mehdad, R.F. Lobo, Ethane and ethylene aromatization on zinc-containing zeolites, Catal. Sci. Technol. 7 (2017) 3562–3572.

[23] Y. Xiang, H. Wang, J. Cheng, J. Matsubu, Progress and prospects in catalytic ethane aromatization, Catal. Sci. Technol. 8 (2018) 1500–1516.

[24] B. Robinson, X. Bai, A. Samanta, V. Abdelsayed, D. Shekhawat, J. Hu, Stability of Fe- and Zn-promoted Mo/ZSM-5 catalysts for ethane dehydroaromatization in cyclic operation mode, Energy Fuels 32 (2018) 7810–7819.

[25] U.V. Mentzel, A.K. Rovik, C.H. Christensen, Co-conversion of ethane and methanol into higher hydrocarbons over Ga/H-ZSM-5, Mo/H-ZSM-5 and Ga-Mo/H-ZSM-5, Catal. Lett. 127 (2008) 44.

[26] A. Hagen, F. Roessner, Ethane to aromatic hydrocarbons: past, present, future, Catal. Rev. 42 (2000) 403–437.

[27] L. Wang, R. Ohnishi, M. Ichikawa, Selective dehydroaromatization of methane toward benzene on Re/HZSM-5 catalysts and effects of CO/CO_2 addition, J. Catal. 190 (2000) 276–283.

[28] H.S. Lacheen, P.J. Cordeiro, E. Iglesia, Structure and catalytic function of Re-oxo species grafted onto H-MFI zeolite by sublimation of Re_2O_7, J. Am. Chem. Soc. 128 (2006) 15082–15083.

[29] H.S. Lacheen, P.J. Cordeiro, E. Iglesia, Isolation of rhenium and ReO_x species within ZSM5 channels and their catalytic function in the activation of alkanes and alkanols, Chem. Eur. J. 13 (2007) 3048–3057.

[30] J. Gao, Y. Zheng, Y. Tang, J.-M. Jehng, R. Grybos, J. Handzlik, I.E. Wachs, S.G. Podkolzin, Spectroscopic and computational study of Cr oxide structures and their anchoring sites on ZSM-5 zeolites, ACS Catal. 5 (2015) 3078–3092.

[31] D.W. Fickel, A.M. Shough, D.J. Doren, R.F. Lobo, High-temperature dehydrogenation of defective silicalites, Microporous Mesoporous Mater. 129 (2010) 156–163.

[32] http://www.zeolyst.com/.

[33] G. Bergeret, P. Gallezot, Particle size and dispersion measurements, in: G. Ertl, H. Knozinger, F. Schuth, J. Weitkamp (Eds.), HandBook of Heterogeneous Catalysis, Viley-VCH, 2008, pp. 738–765.

[34] E.I. Gürbüz, D.D. Hibbitts, E. Iglesia, Kinetic and mechanistic assessment of alkanol/alkanal decarbonylation and deoxygenation pathways on metal catalysts, J. Am. Chem. Soc. 137 (2015) 11984–11995.

[35] I.D. Gay, R.D. Kern, G.B. Kistiakowsky, H. Niki, Pyrolysis of ethylene in shock waves, J. Chem. Phys. 45 (1966) 2371–2377.

[36] P.B. Weisz, Polyfunctional heterogeneous catalysis, Advances in Catalysis, Academic Press, 1962, pp. 137–190.